

The Environmental Dependence of Brightest Cluster Galaxies: Implications for Large-Scale Flows

Michael J. Hudson¹

*Department of Physics & Astronomy, University of Victoria, P.O. Box 3055, Victoria, B.C. V8W 3P6, Canada;
hudson@uvastro.phys.uvic.ca*

and

Harald Ebeling²

Institute of Astronomy, Madingley Road, Cambridge CB3 0HA, UK

ABSTRACT

In a much-noticed recent study Lauer and Postman (1994) found that the inertial frame defined by a sample of 119 nearby Abell clusters with $cz_{\odot} < 15000 \text{ km s}^{-1}$ showed a highly significant motion with respect to the cosmic microwave background (CMB) frame. We construct a subsample of their sample which comprises 64 Abell/ACO clusters with X-ray luminosities from ROSAT and brightest cluster galaxy (BCG) photometry from Lauer and Postman. We find that both BCG metric luminosities and residuals from the $L_m - \alpha$ relation of Lauer & Postman are significantly correlated with the X-ray luminosity of the host cluster at the 99.6% confidence level, in the sense that more X-ray luminous clusters have brighter BCGs. The strength of this correlation increases with increasing X-ray luminosity and with increasing values of the structure parameter α . Taking this correlation into account, we obtain a new distance indicator for BCGs, the $L_m - \alpha - L_X$ relation. Applying the $L_m - \alpha - L_X$ relation to our sample, we find that the frame defined by these clusters has a bulk motion of 494 km s^{-1} towards $l = 285^\circ, b = 47^\circ$ with respect to the CMB frame but the 95% confidence range on the amplitude is 306 to 1419 km s^{-1} . When the covariance of the components of the bulk motion is properly taken into account, these results are inconsistent with this frame being at rest in the CMB frame at the 98.6% confidence level but are consistent with the 300–400 km s^{-1} amplitude flows found by other studies on scales $cz \lesssim 6000 \text{ km s}^{-1}$. In order to obtain an estimate of the bulk flow on scales beyond local perturbations such as the “Great Attractor”, we have also examined the subsample of 57 clusters with X-ray data and $cz_{\text{LG}} > 6000 \text{ km s}^{-1}$. The random errors in the bulk motion are large due to the depth and small size of this sample. We find that the bulk motion of the clusters in this shell with respect to the CMB frame is not statistically significant, but the 95% confidence limits for the amplitude range from 27 to 2025 km s^{-1} . The motion of this sample is

¹CITA National Fellow

²also: Institute for Astronomy, 2680 Woodlawn Drive, Honolulu, HI 96822, USA; ebeling@ifa.hawaii.edu

also consistent with the motion found by Lauer and Postman. However, our analysis of all 107 Lauer and Postman BCGs with $cz_{LG} > 6000 \text{ km s}^{-1}$ indicates that, even with no X-ray correction, the motion of these clusters with respect to the CMB frame is not significantly different from zero. Furthermore, the correction to the bulk motion of the subsample with the X-ray data goes in the sense of reducing the amplitude (by 663 km s^{-1}) and significance (from 98.8% to 83.8%) of its motion in the CMB frame, as well as reducing the internal inconsistency between its motion and that of the remainder of the Lauer and Postman sample with no X-ray data. Claims of large-scale, large-amplitude bulk flows should therefore be regarded with caution until X-ray data become available for more clusters, or cluster distances are confirmed by independent methods.

Subject headings: galaxies: distances and redshifts — galaxies: elliptical and lenticular, cD — galaxies: clusters: general — X-rays: general — cosmology: observations

1. Introduction

Brightest cluster galaxies (BCGs) have been used as cosmological probes since the pioneering work of Sandage and collaborators (Humason, Mayall & Sandage 1956; Sandage 1972a,b). Initially, BCGs were seen as a promising means of measuring q_0 (e.g. Sandage 1972a,b). Recently, BCGs have been used to measure the large-scale streaming motion of the local Universe, with conflicting results (Sandage 1975; James, Joseph & Collins 1987; Lucey & Carter 1988). Lauer & Postman (1994, hereafter LP; Postman & Lauer 1995, hereafter PL), using a sample of BCGs in Abell/ACO clusters (Abell 1958; Abell, Corwin & Olowin 1989) with $cz_{\odot} < 15000 \text{ km s}^{-1}$, found that the inertial frame defined by these clusters (hereafter ACIF) is moving with respect to the cosmic microwave background (CMB) frame at $689 \pm 178 \text{ km s}^{-1}$ which is significant at the greater than 99.99% (4σ) level. Given that a large-scale flow of this amplitude is in conflict with most cosmological models at the 95-99% confidence limit (Strauss *et al.* 1995; Feldman & Watkins 1994; but see also Jaffe and Kaiser 1995), it is clearly important to re-examine this result and, in particular, the corrections applied to the BCG magnitudes as measured.

BCGs are not perfect standard candles and most workers have found that some form of correction to their magnitudes is necessary before they can be used as distance indicators. Sandage (1972a,b) applied both cluster richness and Bautz-Morgan (1970, BM) type corrections to BCG metric luminosities. Hoessel (1980) found that taking into account the correlation between the luminosity L_m within a metric aperture of radius R_m and the logarithmic slope of the luminosity profile at that aperture, $\alpha \equiv (d \log(L_m) / d \log R)|_{R_m}$, led to reduced scatter and eliminated the need for cluster richness or BM corrections. However, Hoessel & Schneider (1985) found that the correction “removes much of the richness and BM – luminosity trends, but perhaps not all.” Finally, LP used an $L_m - \alpha$ relation similar to that of Hoessel (1980), again with no richness or BM corrections, in order to derive the bulk motion of the ACIF. PL showed that there is no correlation between Abell richness and residuals from their $L_m - \alpha$ relation (although a visual examination of their Figure 7d suggests that the BCGs of Richness Class ≥ 2 clusters may have slightly brighter residuals than poorer clusters).

A correlation between the luminosity of the BCG

and the environment of the host cluster may arise for different reasons. For instance, such a correlation may have an astrophysical basis in the sense that BCGs in richer environments grow more easily by cannibalising other cluster galaxies. Alternatively, such a correlation might arise from statistical considerations: if BCGs are simply the brightest members of a population drawn at random from a luminosity function, then clusters with more galaxies will tend to have brighter BCGs (Scott 1957; Peebles 1968). While this distinction is important for understanding the history of galaxy formation and mergers in clusters, it is immaterial for the main purpose of this paper – we are concerned with *any empirical* correlation and its consequences for large-scale motions.

However, the richness or projected galaxy density may not be the most sensitive probe of the cluster environment. In particular, projection effects can cause the two-dimensional richness to be a poor estimator of the true three-dimensional galaxy density around the BCG (Lucey 1983; Sutherland 1988; van Haarlem 1996). Only the latter, however, can be expected to be correlated with the BCG luminosity. Selection of clusters by the X-ray emission from the gaseous intra-cluster medium has several advantages over optical selection. First, the existence of diffuse gas at temperatures of typically 10^{7-8} K guarantees that the cluster is a bound system with a deep potential well. Second, the X-ray emission is unlikely to be contaminated by foreground/background groups which are projected onto the cluster. This is because the X-ray volume emissivity is proportional to the square of the gas density and thus much more peaked than the projected galaxy distribution by which clusters have traditionally been selected and defined at optical wavelengths. Finally, if clusters are selected from different optical catalogues in different hemispheres (e.g. Abell vs. ACO catalogues), then a systematic difference in cluster richness (e.g. Scaramella *et al.* 1991) would bias the bulk motion if the properties of the BCG are indeed correlated with richness. The use of X-ray data from an all-sky survey eliminates all these biases and allows more physical parameters such as the X-ray gas temperature or the X-ray luminosity to be used to parametrise a cluster’s richness. Indeed, Edge (1991) found a strong correlation between the cluster X-ray temperature and BCG magnitudes, and a slightly weaker correlation between X-ray luminosity and BCG magnitude.

The goals of this work are twofold: first, to deter-

mine if BCG photometric properties are correlated with the X-ray luminosities of their host clusters; and second, to investigate the impact of such correlations on the derived large-scale flow field. In Section 2, we introduce the X-ray sample, and in Section 3 we show that a strong correlation of this type does indeed exist. In Section 4, we investigate the implications of this correlation for large-scale flows by performing a simultaneous fit to the parameters of the L_m - α - L_X relation and the motion of the Local Group (LG). Throughout we adopt $H_0 = 80 \text{ km s}^{-1} \text{ Mpc}^{-1}$ and $q_0 = 0.5$ when calculating luminosities, but quote distances in units of km s^{-1} .

2. Data

The sample of the X-ray brightest Abell-type clusters (XBACs) of Ebeling *et al.* (1996) is an X-ray flux-limited ($f_X > 5.0 \times 10^{-12} \text{ erg cm}^{-2} \text{ s}^{-1}$ in the 0.1 – 2.4 keV band) sample of all Abell/ACO (Richness ≥ 0) clusters detected in the ROSAT All-Sky Survey (RASS). 56 of the 119 clusters in the ACIF sample are also contained in the XBACs sample. A further 17 of the clusters in the ACIF sample have been detected in the RASS but fall below the flux limit of the published XBACs sample (Ebeling, private communication). The RASS X-ray luminosities of these additional 17 clusters remain proprietary data of MPE and are not available for this study. A search of the ROSAT data archive, however, uncovered another 12 detections of ACIF clusters in deeper pointings with the PSPC (the same detector that was used during the RASS) thus bringing our total sample of X-ray detected ACIF clusters to 68. Five of these 68 are classified as double clusters in the X-ray. As a comparison between cluster X-ray fluxes from the RASS and fluxes for the same clusters obtained from pointed PSPC observations showed the two data sets to be in excellent agreement (Ebeling *et al.* 1996), we are confident that the merging of cluster detections from the RASS and pointed observations does not introduce any systematic bias. If a cluster from the XBACs sample has also been observed in a PSPC pointing, we adopt the flux from the pointed observation as the latter goes deeper in all cases thus yielding better photon statistics. (We have confirmed that our results are unaffected if we use only the RASS data.) All X-ray fluxes are accurate to typically 10 to 20 per cent and have been corrected for foreground Galactic absorption. Note that the fluxes are dominated by emission from the intracluster medium and not by

individual sources such as, for instance, the BCG or contaminating AGN. In the case of the pointed observations this was ensured by explicitly removing all flux from point sources from the overall emission; for the RASS detections where the photon statistics are usually too poor to allow such an individual treatment a statistical correction was applied to the total cluster emission (see Ebeling *et al.* 1996 for details).

On the optical side, we use the BCG photometry of PL (their Table 3). We fit a quadratic form in $\log(\text{aperture})$ to the tabulated photometry yielding the parameters M_L , α_L (evaluated at the 10 h^{-1} kpc radius aperture assuming the cluster is at rest in the LG frame) and $\alpha' \equiv (d\alpha/d\log R)|_{R_m}$. The derivative α and second derivative α' allow us to determine, by Taylor series expansion, L_m and α for any assumed BCG distance and corresponding 10h^{-1} kpc metric aperture. Extinction and k corrections are as in PL. Of the 68 clusters that our X-ray sample has in common with the ACIF list, we reject the following clusters for which the positions of the BCG and the X-ray centroid were found to be discrepant: A189, a multiple system (Zabludoff *et al.* 1993) in which the BCG of LP corresponds to the group at $cz = 9925 \text{ km s}^{-1}$ while the X-ray centroid is coincident with the foreground system centred on NGC 533 at $cz = 5544 \text{ km s}^{-1}$; A1228, also a multiple system (Zabludoff *et al.* 1993) in which the BCG of LP is in the “A” group at $cz = 10674 \text{ km s}^{-1}$, and the X-ray centroid is centred on UGC 06394 in the “B” group at $cz = 12715 \text{ km s}^{-1}$; A3560 for which the LP BCG is NGC 5193 at $cz = 3644 \text{ km s}^{-1}$ and the main cluster is in the background at $cz = 14840 \text{ km s}^{-1}$ (Vettolani *et al.* 1990); and A3869 in which the LP BCG is NGC 7249 at $cz = 12005 \text{ km s}^{-1}$ and the X-ray centroid is coincident with the cluster APM 222041.3-552848 at $z = 0.078$ (Dalton *et al.* 1994) as also noted by Ebeling *et al.* (1996). In the five cases where two X-ray subclusters are associated with a given Abell/ACO cluster, we use again the component with the best positional agreement with the BCG (A548a, A1631a, A2197b, A2572a and A3528b) in order to ensure that the optical and X-ray parameters used in our study are indeed associated with the same physical system. We refer to the frame defined by this sample as the XACIF (X-ray–Abell cluster inertial frame). Table 1 lists the optical and X-ray properties of the XACIF sample.

Table 1 follows the References.

In our analysis of the bulk motion below, we shall

also consider the statistically independent subsample of clusters for which X-ray data are unavailable, because they have X-ray fluxes below the flux limit of the XBACs sample and have not been observed in PSPC pointings either. We refer to this as the NOX sample. Note that many of the NOX clusters are detected in the RASS, but their fluxes have not been released by MPE.

Figure 1 shows the distribution of clusters on the sky. The clusters with X-ray and without X-ray data are shown by the filled and open circles respectively.

3. The Environmental Dependence of BCGs

Figure 2 shows the correlations between the BCG properties M and α and the host cluster's X-ray luminosity. The top panels of Figure 2 show BCG magnitude as a function of L_X , whereas the lower panels show the residuals from the L_m - α relation, $\Delta M(\alpha)$, as a function of L_X . The sample is subdivided by α : the left panels show the half of the sample with $\alpha < 0.64$, the middle panels show the quartile with $0.64 \leq \alpha < 0.77$ and the right panels show the top quartile ($\alpha \geq 0.77$). The data in the XACIF sample are indicated by solid circles. BCGs for which we have only upper limits on the cluster X-ray luminosity are indicated by horizontal arrows. The dashed lines show the best fit to each subsample. Note that the X-ray coverage of the ACIF sample is essentially complete for high X-ray luminosity/high α systems. It is clear that for large α both M and $\Delta M(\alpha)$ are significantly correlated with L_X . Linear and rank correlation statistics applied to the detections indicate that this correlation is significant at the $\gtrsim 95\%$ level for $\alpha \gtrsim 0.6$. The significance of these correlations remains the same whether we assume that the ACIF is at rest with respect to the LG or to the CMB frame. It should also be noted that this correlation is not the result of peculiar velocities perturbing both L_X and $\Delta M(\alpha)$ since a typical peculiar velocity of 500 km s^{-1} at a distance of 10000 km s^{-1} changes $\log(L_X)$ by only 0.042 and ΔM by ~ 0.075 mag.

In order to assess whether these correlations remain significant when we include upper limits, we have calculated the generalized Kendall's τ statistic (Isobe, Feigelson and Nelson 1986) using the ASURV package, Rev 1.2 (available from code@stat.psu.edu). This statistic tests for the existence of a rank correlation allowing for one or both variables to be limits or detections. When we cut the sample, we find signifi-

cant ($\geq 95\%$) correlations for all subsamples for which $\alpha_{\min} \geq 0.6$. In fact, the correlation for the complementary $\alpha < 0.6$ subsample is marginally significant (at the 93.3% confidence level).

Similar to PL's Figure 1 our Figure 3 shows the L_m - α diagram of the ACIF sample with the clusters with and without X-ray information plotted as filled and open circles respectively. In order to compare the properties of BCGs with those of cluster giant ellipticals, we have mapped the ellipticals in Coma (Lucey *et al.* 1991) onto the L_m - α diagram assuming that they follow an $R^{1/4}$ law and adopting a mean colour of $V - R_c = 0.56$. Also plotted is the Kormendy (1977) relation (a projection of the Fundamental Plane) of Guzman *et al.* (1993) for the same galaxies. Note the good continuity between the distribution of giant ellipticals and the lower α half of the LP BCG sample. The Kormendy relation appears to be an acceptable fit to both giant ellipticals and BCGs up to $\alpha \sim 0.55$, whereas for higher values of α the L_m - α relation deviates from the Kormendy relation. Also, it appears from Figure 2 that, for $\alpha \lesssim 0.6$, the L_m - α residuals do not correlate strongly with the X-ray luminosity of the host cluster, whereas above this value we find an increasingly strong dependence on L_X . Finally it is worth noting that there also exists a highly significant correlation between α and L_X in the sense that larger α galaxies are found in more X-ray luminous clusters. A simple interpretation of all the above observations is that low- α BCGs are typically found in low L_X (and hence typically poor) clusters and follow the same Fundamental Plane relations as lower-ranked cluster ellipticals independent of the cluster environment. High- α BCGs, on the other hand, are typically found in rich clusters and have photometric properties which depend on the cluster's X-ray luminosity and presumably on its mass.

To summarize, we have shown that, for large α ($\gtrsim 0.6$) BCGs, there is a significant correlation between both the BCG magnitudes themselves and the residuals of the L_m - α relation and L_X . For small α ($\lesssim 0.6$) BCGs, the correlation between residuals of the L_m - α relation and L_X is only marginally significant (at the 93.3% confidence level) and, in any case, weaker than that found for the large- α BCGs. The X-ray correction to an individual BCG aperture magnitude can be quite large (e.g. ~ 0.5 mag for the X-ray luminous cluster A3571). A difference between the mean X-ray luminosities of clusters on opposite sides of the sky could thus translate into a spurious

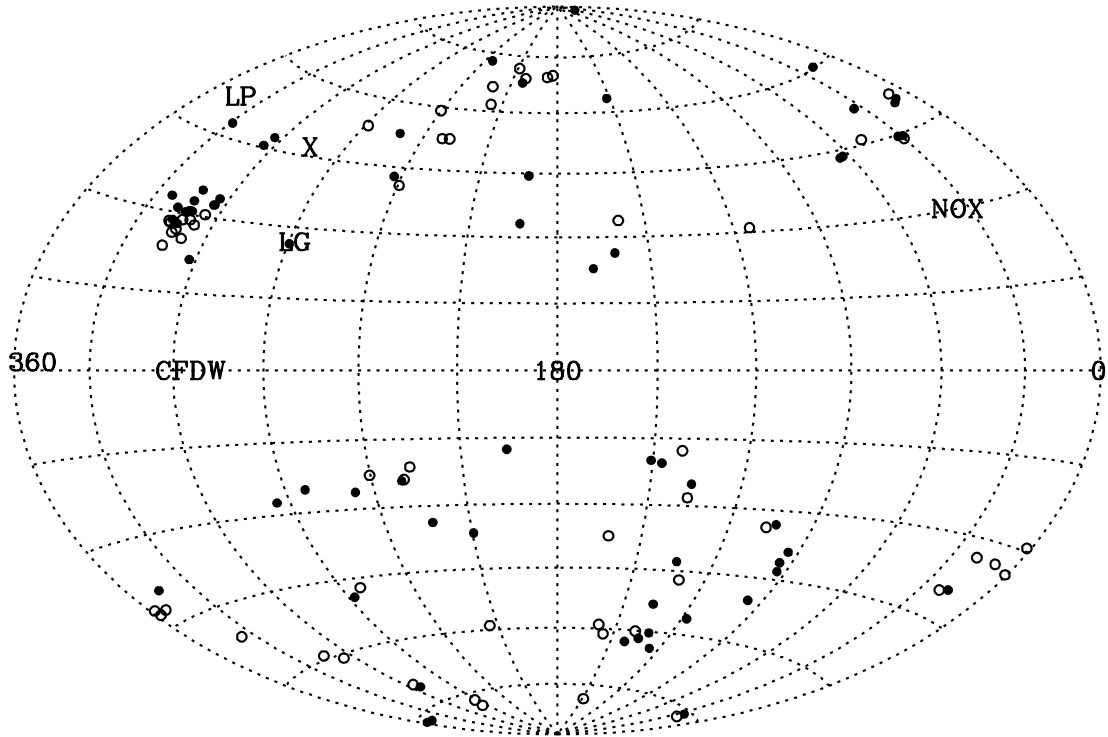


Fig. 1.— The distribution of clusters on the sky in an Aitoff projection of Galactic coordinates. Clusters with and without X-ray data are indicated by the filled and open circles respectively. The labels give the directions of the bulk motion in the CMB frame for samples of LP (indicated by “LP”), and Courteau *et al.* 1993 (“CFDW”), for the XACIF (“X”) and NOX samples (“NOX”) discussed in Section 4, and for the Local Group (“LG”).

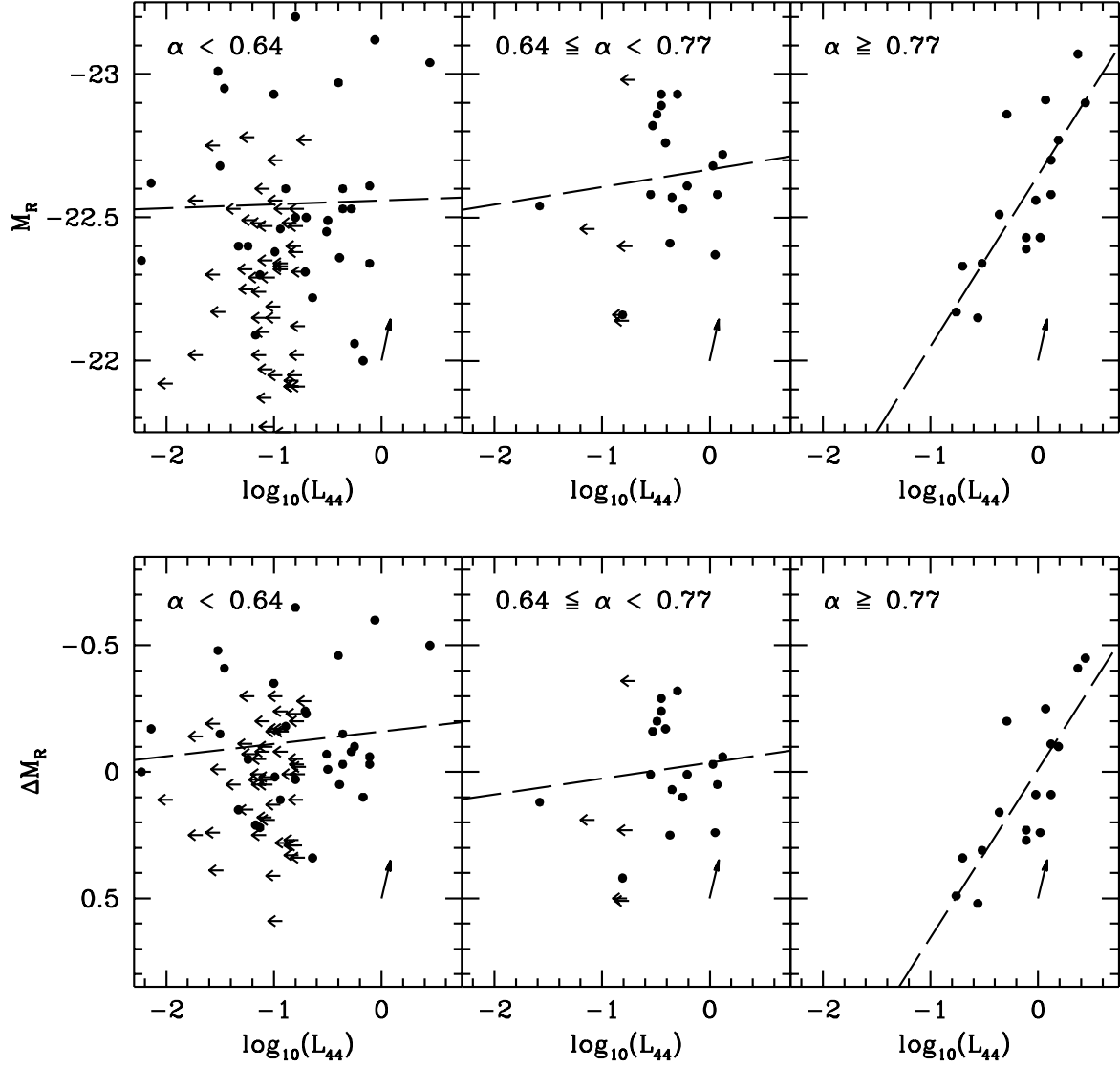


Fig. 2.— The correlations between the BCG properties M and α and the host cluster's X-ray luminosity (LG frame). The top panels show BCG metric magnitude as a function of $\log(L_{44})$ whereas the lower panels show the residuals from the $L_m-\alpha$ relation, $\Delta M(\alpha)$, as a function of $\log(L_{44})$. The data in the XACIF sample are indicated by solid circles. BCGs for which we have only upper limits on the cluster X-ray luminosity are indicated by horizontal arrows. The sample is subdivided by α : the left panels show the half of the sample with $\alpha < 0.66$, the middle panels show the second quartile with $0.64 \leq \alpha < 0.77$ and the right panels show the top quartile ($\alpha \geq 0.77$). The dashed lines show the best fit to the BCGs with X-ray detections in each subsample. The correlation found for high values of α is highly significant. The arrow on the lower right of each panel indicates the change in parameters if the distance of a cluster is increased by 10% (twice the typical error due to peculiar velocities).

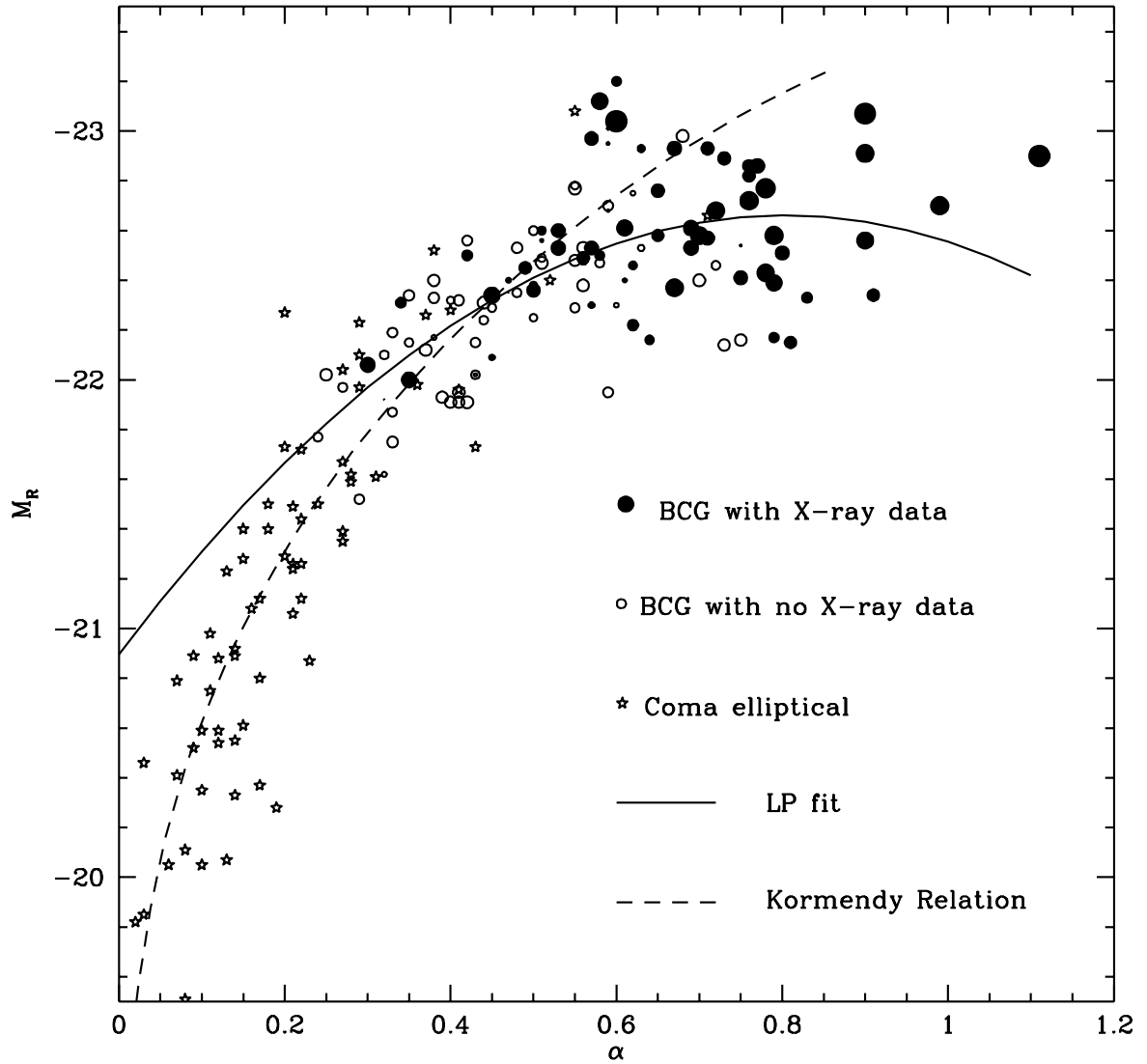


Fig. 3.— The L_m – α relations for BCGs and giant ellipticals. Filled circles are BCGs in clusters with X-ray data and open circles are BCGs with no X-ray data. The radius of the circle is proportional to $\log L_{42}$ (the measured X-ray luminosity or the upper limit, for filled and open circles respectively). Ellipticals in Coma are indicated by stars. These have been mapped onto the M_R – α diagram by assuming that they have $R^{1/4}$ law profiles. The solid line is the L_m – α relation of LP. The dashed curve is the projection of the Kormendy relation followed by giant elliptical galaxies.

bulk flow if the X-ray correction is neglected.

4. The Bulk Motion

4.1. Method

In order to investigate the effects of the X-ray correlation on the derived bulk flow, it is necessary to determine a L_m - α - L_X relation and re-derive the motion of the sample. We fit simultaneously both the parameters of the L_m - α - L_X relation, denoted by \mathbf{c} , and the motion of the LG with respect to the sample, \mathbf{L} . Our method of fit is to minimize the aperture magnitude residuals (Colless 1995)

$$\chi^2 = \sum_i^N \left(\frac{\Delta M(r_i(\mathbf{L}), \mathbf{c})}{\sigma_m(r_i(\mathbf{L}))} \right)^2 \quad (1)$$

simultaneously as a function of \mathbf{c} and \mathbf{L} . Note that the motion of the LG with respect to the XACIF sample fixes the distance (in units of km s^{-1}), r_i , of each BCG via the relation $r_i = cz_{\text{LG},i} + \mathbf{L} \cdot \hat{\mathbf{r}}_i$, where $z_{\text{LG},i}$ is the observed redshift of the i^{th} cluster in the LG frame.

The residuals from this fit are given by

$$\Delta M(r, \mathbf{c}) = M(r) - \overline{M(r, \mathbf{c})} \quad (2)$$

where the predicted magnitude is

$$\begin{aligned} \overline{M(r, \mathbf{c})} = & c_0 + c_1 \alpha + c_2 \alpha^2 + c_3 \log(L_{44}) \\ & + c_4 \alpha \log(L_{44}) + c_5 \alpha^2 \log(L_{44}). \end{aligned} \quad (3)$$

L_{44} is the cluster X-ray luminosity in units of 10^{44} ergs s^{-1} in the $0.1 - 2.4$ keV band. Note that M , α and $\log(L_{44})$ are all non-linear functions of r and hence of \mathbf{L} .

For the NOX sample (for which X-ray data are unavailable) we follow an identical procedure to that described above, except that we use an L_m - α relation of the same functional form as LP, i.e. we set c_3 , c_4 and c_5 equal to zero. For completeness we also rederive the motion of the original ACIF sample neglecting all X-ray data and using the L_m - α relation.

The total scatter in magnitudes is $\sigma_m^2 = \sigma_0^2 + \left(\frac{d\Delta M}{dr} \sigma_v \right)^2$, where σ_0 is the intrinsic scatter in magnitudes about the L_m - α - L_X relation, and σ_v is the dispersion in peculiar velocity around the best-fitting flow model. This scatter in velocity arises from two sources. Firstly, we have peculiar velocities due to structures within the sampled volume that are not

accounted for because we model the flow as a simple bulk motion. Gramann *et al.* (1995) estimate the one-dimensional velocity dispersion of clusters to be approximately 300 km s^{-1} . Secondly, there will be a contribution from observational errors in the cluster redshifts. LP estimate the errors in measured redshift to be approximately 184 km s^{-1} . Adding these in quadrature, we adopt $\sigma_v = 350 \text{ km s}^{-1}$. The velocity scatter contributes to the σ_m of nearby clusters but is negligible for the more distant clusters for which the error is dominated by σ_0 . Our final results are not very sensitive to the choice of σ_v .

Using equation 2, it is straightforward to calculate the change in magnitude residuals for a given change in log distance.

$$\frac{d\Delta M}{d \log r} = \frac{dM(r)}{d \log r} - \frac{d\overline{M(r, \mathbf{c})}}{d \log r} \quad (4)$$

with

$$\frac{dM(r)}{d \log r} = -2.5 [2 - \alpha] \quad (5)$$

and

$$\begin{aligned} \frac{d\overline{M(r, \mathbf{c})}}{d \log r} = & -\alpha' [c_1 + 2c_2 \alpha + c_4 \log(L_{44}) \\ & + 2c_5 \alpha \log(L_{44})] \\ & + 2 [c_3 + c_4 \alpha + c_5 \alpha^2] \end{aligned} \quad (6)$$

where we have used $d\alpha/d \log r = -\alpha'$ and $d \log L_{44}/d \log r = 2.3$.

³ While the calculation of the magnitude residual (equation 2) is always performed relativistically, the expressions for the derivatives (equations 5 & 6) neglect relativistic terms which arise from (a) the change in luminosity with redshift and (b) the change in the angular diameter of the $10h^{-1}$ metric aperture. For a typical BCG the change in $M(r)$ due to the relativistic terms over the typical distance error is 0.008 mag (to be compared with the L_m - α scatter of 0.244 mag). The effect of including the relativistic terms would be to reduce the estimated errors, but due to the low mean redshift ($z \sim 0.025$) of the sample, the effect on the fractional distance error is small: a factor ~ 0.97 .

As the distance of a galaxy changes, its position in the L_m - α diagram changes too. We approximate its true path, which is mildly parabolic, by a straight line. This is valid if the distance errors are small. For the typical galaxy the change in magnitude residual due to this second-order term is very small: 0.002 mag, two orders of magnitude smaller than the scatter 0.244 mag. Furthermore, since this correction can have either sign depending on whether the distance is over- or underestimated, it will tend to cancel out. We are therefore justified in neglecting this second-order term.

The fractional distance error is then given by

$$\sigma_r = \ln(10) \left(\frac{d\Delta M}{d \log r} \right)^{-1} \sigma_0 \quad (7)$$

and the peculiar velocity error is the quadrature sum of the distance error and σ_v . Note that α is a distance-dependent quantity. For an $R^{1/4}$ profile, α is monotonically related to $\log R_e$ (Graham *et al.* 1996). When calculating their peculiar velocity *errors* LP considered only equation (5) corresponding to the change in the *observed* aperture magnitude with distance. However, because α is a (weakly) distance-dependent variable it is important not to neglect the $d\alpha/d \log r = -\alpha'$ terms which correspond to the change in the *predicted* magnitude as a function of distance (i.e. equation 6).

For nearly all of the BCGs in the ACIF sample, the result of including this term is that the distance error increases. This is particularly important at low α where the slope of the $L_m-\alpha$ relation is steep, and hence the change in predicted magnitude for a change in α is large. For example, consider a small $\alpha = 0.3$ galaxy with a typical value of $\alpha' = -0.5$. Using the parameters of LP's $L_m-\alpha$ relation, LP's equation (2) gives a distance error of 13% whereas equation (7) gives an error of 23% (neglecting the X-ray dependent terms). Consequently, in our analysis of the ACIF sample the mean distance error is 18.7% with an rms of 6%, roughly independent of α , whereas LP's α -dependent distance error has a mean of 15.8%⁴. The net result is that while our ACIF \mathbf{L} agrees with LP's value, the *errors* on the three components are systematically slightly larger than those quoted by LP. We have confirmed that, if we neglect the distance dependence of α by setting α' to zero, we obtain the smaller errors of LP.

The X-ray luminosity is also a distance-dependent quantity, and we find that the $L_m-\alpha-L_X$ relation steepens for large L_X . (Note that in Figure 2, the line of best fit steepens and becomes closer in slope to the arrow indicating the effect of distance errors.) Consequently, very large α BCGs in the most X-ray luminous clusters are poor distance indicators. The

⁴ For the mean redshift ~ 0.025 , the effect of including relativistic terms discussed in the previous footnote is to reduce our $L_m-\alpha$ fractional error from 18.7% to 18.2%. When one outlying BCG (A3374) with large distance error is excluded, the mean fractional distance error is 17.7%, in good agreement with the scatter of 17.3% obtained by comparing estimated redshifts with observed redshifts on a galaxy-by-galaxy basis (PL).

distance error for the $L_m-\alpha-L_X$ relation is typically in the range from 11% to 35% with a median of 17%.

For the χ^2 minimization (equation 1), the effective weight of a BCG in the bulk flow solution is proportional to the inverse square of its peculiar velocity error, which is the fractional error (equation 7) times the BCG distance. Thus, for our solutions, high and low α galaxies contribute with approximately equal weights, and the weight drops with distance approximately as r^{-2} . The exceptions are the very large α BCGs in the most X-ray luminous clusters, which, by virtue of their large fractional errors, have low weight.

In order to determine σ_0 , we fix σ_v and adjust σ_0 so that (for the best-fitting solution) we obtain χ^2 equal to the number of degrees of freedom (the number of clusters less the nine free parameters). This yields $\sigma_0 = 0.231$, which is less than the value 0.253 obtained when we fit the $L_m-\alpha$ relation to the same 64 clusters. (The σ_m of 0.244 found by LP for the $L_m-\alpha$ relation alone was for all 119 clusters. However, LP noted that the scatter increases for the $\alpha < 0.6$ subsample where most of the clusters in the XACIF sample are found.) We adopt $\sigma_0 = 0.231$ in order to evaluate the errors on the parameters. For the best-fit solution, the parameters are $c_0 = -21.219$, $c_1 = -4.046$, $c_2 = 2.783$, $c_3 = -1.605$, $c_4 = 5.724$, $c_5 = -5.139$. Figure 4 compares the $L_m-\alpha-L_X$ relation to the $L_m-\alpha$ relation of LP.

If we set c_3 , c_4 and c_5 to zero, thereby ignoring the X-ray data, we find that χ^2 increases by 13.5 for an increase of only 3 in the number of degrees of freedom. This check confirms that the correlation with X-ray luminosity is highly significant (99.6% confidence). Indeed, it is worth noting that the reduction in χ^2 due to the X-ray correction, parametrized by the c_3 , c_4 and c_5 , is far more significant than that due to the choice of bulk flow, parametrized by the three components of \mathbf{L} , as will be shown below.

4.2. Monte Carlo Experiments

To assess whether the geometry of the XACIF sample biases the flow solution, we have performed Monte Carlo (MC) experiments with mock data for the XACIF data sample. For each such mock data set, we use the measured position, redshift and profile shape (which determines α and its derivative for any distance) of each BCG in the XACIF sample, assume a bulk flow and parameters of the $L_m-\alpha-L_X$ relation, and then randomly generate X-ray luminosities

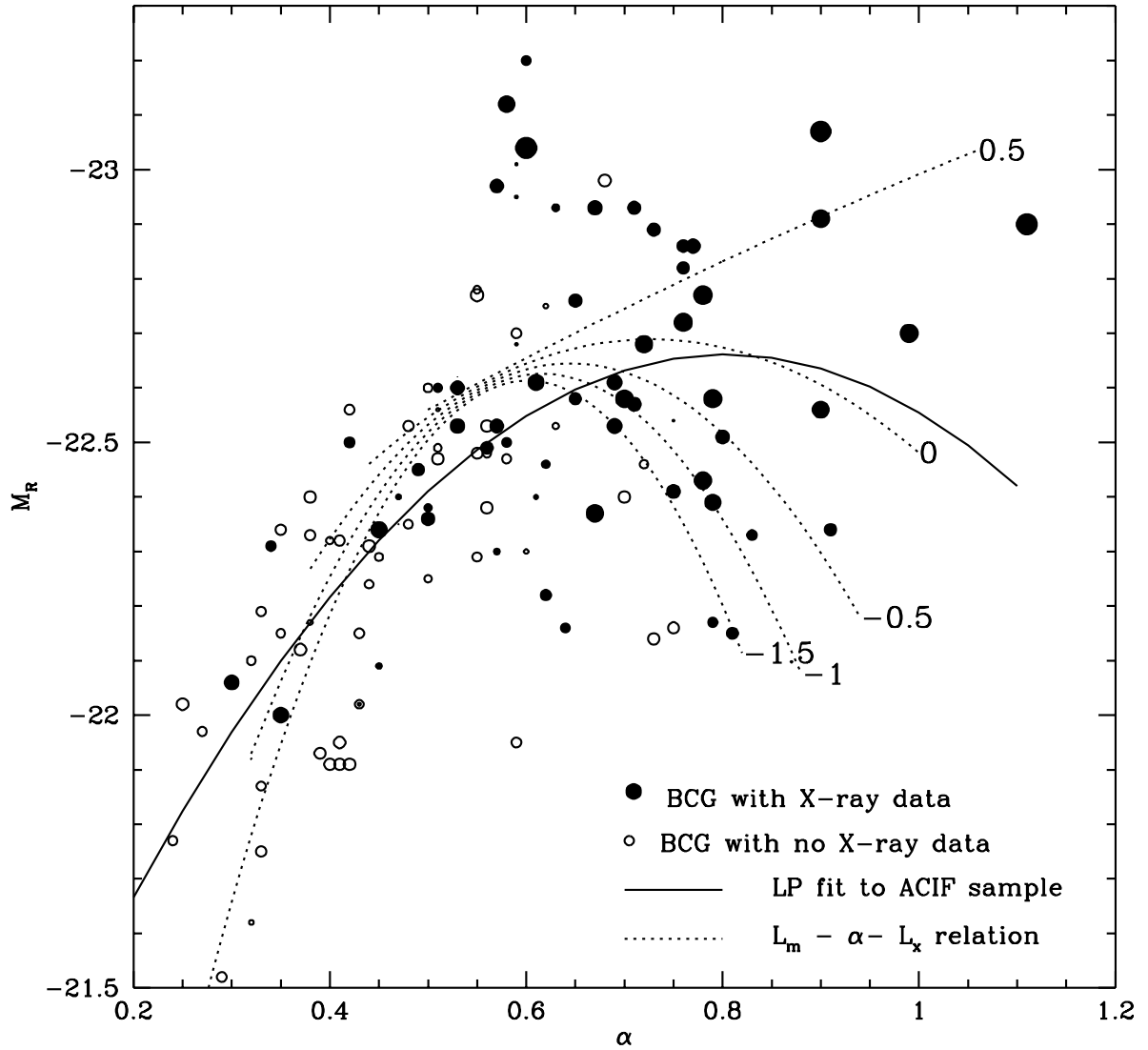


Fig. 4.— The $L_m - \alpha$ and $L_m - \alpha - L_X$ relations for BCGs. Filled circles are BCGs in clusters with X-ray data and open circles are BCGs with no X-ray data. The radius of the circle is proportional to $\log L_{42}$ (the measured X-ray luminosity or the upper limit for filled and open circles respectively). The solid line is the $L_m - \alpha$ relation of LP. The dotted curves show the $L_m - \alpha - L_X$ relation for values of $\log(L_{44})$ ranging from -1.5 to 0.5.

using the $\alpha-L_X$ relation and aperture magnitudes using the $L_m-\alpha-L_X$ relation. We find that the scatter in the bulk flow parameters from one MC realization to another is in excellent agreement with the errors inferred from our χ^2 minimization. We find only a very small level of “geometry bias” in our recovered flow solutions: the results differ from the input values by typically 10–20 km s $^{-1}$ in each component. This is a factor ~ 20 smaller than the random errors.

We have also examined whether our results are affected by a Malmquist-like bias due to the X-ray flux limit. Since the ACIF is believed to be volume-limited, we can use it as the underlying cluster density field from which X-ray flux-limited samples are drawn. We assign X-ray luminosities and aperture magnitudes as described above to the entire ACIF sample and then impose a flux limit which matches that of the XBACs sample in order to generate mock XACIF samples. The resulting bias, which includes both Malmquist and geometry biases, is at the 10–20 km s $^{-1}$ level. We conclude that for our analysis both geometry and Malmquist biases are small and so can be neglected.

4.3. Bulk Flow Results

Table 2 gives the solutions for the motion of the LG, \mathbf{L} , in Galactic Cartesian coordinates with respect to the XACIF, NOX and ACIF samples. The directions of the bulk flow motions found for the respective samples are marked in Figure 1.

Converting the motion of the LG with respect to the sample to the motion of the sample with respect to the CMB, we find that the XACIF clusters have a motion of 867 km s $^{-1}$ towards $l = 285^\circ$, $b = 47^\circ$ in the CMB frame. However, as noted by LP, the amplitude of the flow is biased upwards by the random errors. After correction for “error biasing” by subtracting the errors from the observed amplitude in quadrature, the best estimate of the amplitude of the bulk flow is in the CMB frame is 494 km s $^{-1}$, but the 95% confidence range on the amplitude is 306 to 1419 km s $^{-1}$. In contrast, the error-bias corrected bulk motion of the NOX sample is 1183 km s $^{-1}$ towards $l = 35^\circ$, $b = 30^\circ$, but again the range in amplitude is large: 339 to 2403 km s $^{-1}$. We caution that the one-dimensional errors quoted above are given only to indicate the approximate level of the random errors. They should *not* be used to compare the motions of the different subsamples or to assess the significance of the motion with respect to the CMB frame. The

proper way to perform such comparisons is to use the full covariance matrices of the errors, as described in Section 4.4 below.

Clusters within 6000 km s $^{-1}$ carry a very large weight in the fits, and are predominantly located in two superclusters (Hydra-Centaurus and Perseus-Pisces), where peculiar velocities may be particularly high. Furthermore, this volume is known to have a mean bulk motion of 360 ± 40 km s $^{-1}$ (Courteau *et al.* 1993, hereafter CFDW). In order to obtain an independent estimate of the bulk motion on large scales, we also analyze samples with $cz_{\text{LG}} > 6000$ km s $^{-1}$ which we refer to as the outer shell. For the XACIF sample in the outer shell, we obtain a motion of 492 km s $^{-1}$ towards $l = 258^\circ$, $b = 37^\circ$, but now the 95% range in amplitude is very large: 27 to 2025 km s $^{-1}$. If, for the same sample, the $L_m-\alpha$ relation obtained from the full ACIF sample is used as a distance indicator, we obtain a motion of 1155 km s $^{-1}$ towards $l = 266^\circ$, $b = 31^\circ$, with a 95% lower limit on the amplitude of 480 km s $^{-1}$. The vector corresponding to the X-ray correction has an amplitude of 455 km s $^{-1}$ in the direction $l = 281^\circ$, $b = 17^\circ$ (close to the direction of the flow in the CMB frame). Clearly, for the outer shell, the X-ray correction has made a large difference to the amplitude and significance of the inferred flow. The NOX sample in the outer shell also appears to show evidence of motion: the 95% lower limit on its amplitude is 303 km s $^{-1}$ towards $l = 39^\circ$, $b = 22^\circ$ (110° from the XACIF motion). The difference vector between the XACIF and NOX outer shell bulk motions has an amplitude of 1998 ± 810 km s $^{-1}$. Note that the XACIF and NOX motions disagree strongly in their X and Y components which differ by 1169 km s $^{-1}$ and 1617 km s $^{-1}$ respectively. On the other hand, the Z components, which disagree with CFDW, agree well with each other. If, instead, we use the $L_m-\alpha$ relation obtained from the full ACIF sample, the disagreement between the bulk motions of the XACIF and NOX subsamples in the outer shell is even worse: the bulk motions differ by 2306 ± 846 km s $^{-1}$.

4.4. The Statistical Significance and Consistency of the Flow Solutions

4.4.1. Independent Samples

In order to assess whether our results are consistent with independent samples and with various assumed flow models (e.g. one in which the sample is at rest in

TABLE 2
BULK FLOW SOLUTIONS

Sample	Fit ^a	σ_0	N	r_{eff}^b km s ⁻¹	L_x^c km s ⁻¹	L_y^c km s ⁻¹	L_z^c km s ⁻¹	$ \mathbf{F} ^d$ km s ⁻¹	l^d	b^d
Full redshift range										
XACIF	XF	0.231	64	7356	-175 ± 462	22 ± 390	-361 ± 365	494⁺⁹²⁵₋₁₈₈	285	47
XACIF	NXA	0.243	64	7684	-207 ± 458	118 ± 403	-378 ± 372	618 ⁺⁸⁸⁸ ₋₂₃₄	286	43
NOX	NXF	0.203	55	8327	-984 ± 368	-1227 ± 490	-414 ± 322	1183 ⁺¹²²⁰ ₋₈₄₄	35	30
ACIF	NXF	0.243	119	8031	-521 ± 303	-353 ± 339	-303 ± 250	593 ⁺⁶⁷³ ₋₂₈₂	339	47
$cz_{\text{LG}} > 6000 \text{ km s}^{-1}$										
XACIF	XF	0.238	57	10373	144 ± 566	254 ± 575	-356 ± 399	492⁺¹⁵³³₋₄₆₅	258	37
XACIF	NXA	0.243	57	10507	63 ± 549	682 ± 543	-489 ± 389	1155 ⁺¹²⁵¹ ₋₆₇₅	266	31
NOX	NXF	0.205	50	10209	-1025 ± 471	-1363 ± 566	-270 ± 341	1153 ⁺¹³⁶⁵ ₋₈₅₀	39	22
ACIF	NXF	0.246	107	10434	-428 ± 392	-267 ± 436	-246 ± 271	308 ⁺¹⁰³⁷ ₋₂₂₁	326	46

^aFits are coded as follows: XF — L_m - α - L_X relation, parameters free; NXF — L_m - α relation parameters are free; NXA — L_m - α relation, parameters are fixed to those of the ACIF solution

^bThe effective depth of the sample.

^cThe motion of the Local Group with respect to the cluster sample.

^dMotion of sample in the CMB frame. The amplitude quoted has been “error-bias corrected”. Errors represent the 95% range in the raw amplitude with the direction fixed. Note that these errors should not be used to determine whether the flow is compatible with a given model. This can only be accomplished with the full covariance matrix.

the CMB frame), it is necessary to use the full covariance matrix of the bulk motion errors. To compare two independent samples, with motions \mathbf{L}_1 and \mathbf{L}_2 , and corresponding covariance matrices \mathbf{C}_1 and \mathbf{C}_2 , we calculate

$$\chi^2 = (\mathbf{L}_1 - \mathbf{L}_2)^T (\mathbf{C}_1 + \mathbf{C}_2)^{-1} (\mathbf{L}_1 - \mathbf{L}_2) \quad (8)$$

and compare the result to a χ^2 distribution with 3 degrees of freedom. Note that when comparing two peculiar velocity samples with different sky coverage and effective depth, we do not expect the measured bulk flows, \mathbf{L}_1 and \mathbf{L}_2 , to be identical even in the limit of no measurement errors due to the different window functions (cf. Watkins & Feldman 1995). Therefore, the confidence with which we conclude that two samples are inconsistent will in general be slightly overestimated. However, in the specific case of the comparison between the XACIF and NOX samples discussed below, it is worth noting that the volumes sampled are very similar in depth and sky coverage (see Table 2 and Figure 1), therefore we expect these samples to partake of the same bulk flow. If we wish to test the hypothesis that, for example, a given sample is at rest with respect to the CMB frame, then \mathbf{C}_2 is set to zero

and \mathbf{L}_2 is set to the motion of the LG with respect to the CMB frame. Table 3 compares the consistency of the motion of the XACIF, NOX and ACIF samples with the CMB frame and with the motion found by CFDW.

The first result of this analysis is that we reject the hypothesis that the XACIF sample is at rest with respect to the CMB frame at the 98.6% (2.5 σ) confidence level. However, this is not surprising given the fact that the motion of this sample is dominated by clusters at a typical distance of only 7300 km s⁻¹, and the fact that the local volume to 60 h⁻¹ Mpc is known to have a ~ 350 km s⁻¹ bulk motion (CFDW). In fact the XACIF motion is consistent with the bulk motion found by CFDW.

On the largest scales, for the outer shell ($cz_{\text{LG}} > 6000$ km s⁻¹), there is no significant (83.8%) evidence of bulk motion with respect to the CMB frame, although for this shell the random errors are large (400 – 600 km s⁻¹ per vector component). Despite these large errors, note that had we neglected the X-ray correction and used instead the L_m - α relation derived from the whole ACIF sample as a distance indicator, we would have concluded that the XACIF clusters in

TABLE 3
STATISTICAL COMPARISON OF FLOW SOLUTIONS

	Fit ^a	P_{CMB}^b	P_{CFDW}^c	P_{NOX}^d
Full redshift range				
XACIF	XF	0.014	0.142	0.185
XACIF	NXA	0.005	0.078	0.231
NOX	NXF	0.032	0.050	
ACIF	NXF	0.004	0.063	
$cz_{\text{LG}} > 6000 \text{ km s}^{-1}$				
XACIF	XF	0.162	0.312	0.098
XACIF	NXA	0.012	0.053	0.046
NOX	NXF	0.079	0.062	
ACIF	NXF	0.114	0.247	

NOTE.—Probability that two given flow solutions are consistent.

^aFits are coded as in Table 2

^bThe probability that the sample is a rest with respect to the CMB frame.

^cThe probability that the sample has the motion found by Courteau *et al.* (1993).

^dThe probability that X-ray selected sample agrees with the solution of the corresponding NOX sample.

the outer shell sample had a highly significant (98.8% confidence) motion with respect to the CMB frame.

In order to further investigate the effect of the X-ray correction on the derived bulk flows, we compare the statistically independent XACIF and NOX samples. (It is not valid to compare, for example, the motion of XACIF sample with that of either the full ACIF sample or that the XACIF clusters using the $L_{m-\alpha}$ relation because these samples are not independent, but see below for further discussion of this issue.) We remind the reader that a significant correlation between BCG magnitude and L_X was found for the (on average more X-ray luminous) clusters in the XACIF sample, whereas a much weaker dependence on the X-ray luminosity of the host cluster is expected of the optical properties of the BCGs in the (on average much less X-ray luminous) clusters in the NOX sample (cf. Figure 2). Under the null hypothesis that the X-ray correction is unimportant, we thus expect the XACIF and NOX samples to obey the same $L_{m-\alpha}$ relation and to yield independent and mutually consistent estimates of the bulk flow. However, when we compare the bulk motions of the XACIF and NOX samples using the $L_{m-\alpha}$ relation derived from the whole sample, we find that in the outer shell the bulk motions are mutually inconsistent at the 95.4% confidence level. The X, Y and Z components of the bulk motions differ by 884, 2111 and 284 km s^{-1} respectively. Given that LP found no significant disagreement when they cut the sample by α or redshift, the XACIF–NOX disagreement highlights the importance of X-ray selection and the resulting correction to the derived bulk flow.

We now consider solutions for the XACIF motion using the $L_{m-\alpha}-L_X$ relation, which allows us to correct for the X-ray dependence of the sample. For the NOX sample, we allow the parameters of the $L_{m-\alpha}$ relation to be free. This does not remove all of the X-ray dependence of this sample, but allows us to make a correction to the mean X-ray luminosity of the sample (which must be lower than that of the XACIF sample given that most of the XACIF clusters were drawn from an X-ray flux limited sample). As noted above, for the outer shell, the XACIF motion is now consistent with being at rest in the CMB frame. The discrepancy between the XACIF and NOX bulk motions is still present but its significance is reduced to the 90.2% confidence level. We suggest that this remaining small discrepancy is caused by the lack of X-ray correction in the solution for the NOX sample

which, owing to its low content in high- α BCGs, is, however, less strongly affected than the XACIF sample.

4.4.2. Correlated Samples

We would also like to assess the statistical significance of the difference between the bulk flow of the XACIF sample with and without the X-ray correction applied, and the difference between the motion of the XACIF sample and that of the ACIF sample. These comparisons cannot be made using the methods described above because these samples are not independent. Indeed, for the XACIF sample, the residuals from the $L_{m-\alpha}$ and $L_{m-\alpha}-L_X$ relations are highly correlated. The simplest way to properly account for this correlation is to use the Monte Carlo (MC) simulations described above. In these simulations, we assume a bulk motion and $L_{m-\alpha}-L_X$ relation, and generate MC realizations of the cluster X-ray luminosities and BCG magnitudes. We can then calculate bulk flows for each MC realization both with and without the X-ray data included in the fit. This allows us to determine the covariance matrix of the vector difference between two bulk flow solutions in a way which accounts for the correlated residuals.

We find that the observed vector difference between the ACIF and X-ray corrected XACIF motions in the outer shell is consistent with the MC covariance matrix derived from the differences between the bulk motion of mock ACIF realizations (using the $L_{m-\alpha}$ relation) and the bulk motion of flux-limited X-ray subsamples (using the $L_{m-\alpha}-L_X$ relation). Therefore, we conclude that, in the outer shell, the X-ray corrected bulk motion of the XACIF sample is consistent with that derived from the ACIF sample without any X-ray correction.

When we compare the bulk flow vectors of MC XACIF realizations with and without the X-ray term, we find that vector differences of amplitude $\sim 500 \text{ km s}^{-1}$ are not uncommon. These vector differences, however, are randomly oriented with respect to the bulk motion vector in the CMB frame, as expected since, in the MC simulations, the cluster X-ray luminosities are uncorrelated with the clusters' positions on the sky. For the actual XACIF sample, however, the vector difference is nearly opposite in direction to the sample's motion in the CMB frame, with the result that the amplitude of the flow, which is 1155 km s^{-1} before the X-ray correction is applied, is reduced to 492 km s^{-1} when the X-ray data are in-

cluded. Such a large reduction in amplitude occurs in $\sim 25\%$ of all cases in the MC simulations but such good alignment occurs in only 2.5% of all cases. We interpret this as evidence that the high amplitude motion (1153^{+1251}_{-675} km s $^{-1}$ where the errors give the 95% range) of the XACIF sample obtained with the L_m – α relation alone (i.e. without the X-ray correction) is systematically biased.

4.5. Discussion

We have shown that the X-ray correction to the BCG L_m – α relation is statistically significant and that the motion of the XACIF sample in the outer shell ($cz_{LG} > 6000$ km s $^{-1}$) is consistent both with no motion with respect to the CMB and with the motion of the ACIF sample found by LP. The implications of this correlation for large-scale flows can only be properly addressed when X-ray data become available for the whole ACIF sample. Given the fact that, while these data exist, they are presently unavailable for almost half of the clusters in the ACIF sample, how do we interpret our results?

The conservative approach is to assume that, given the relevance of the X-ray correction, one can safely use as distance indicators only those BCGs that have measured cluster X-ray luminosities, and hence that, on large scales, the flow solutions are consistent with the most conservative interpretation that these systems are at rest in the CMB frame.

On the other hand, an unfortunate consequence of the small size of the XACIF sample is that the errors on the bulk motion are large so that we also cannot reject the (albeit less conservative) hypothesis that there is a ~ 600 km s $^{-1}$ bulk flow as found by LP. The following facts, however, argue against the existence of large-amplitude flows beyond 6000 km s $^{-1}$. Firstly, the L_m – L_X distance indicator reduces the amplitude of the XACIF flow by 663 km s $^{-1}$ and brings the XACIF sample into better agreement with the CMB frame compared to the L_m – α relation applied to the same BCGs. A reduction of this amplitude is unlikely to occur if the X-ray correction vector is randomly oriented with respect to the motion, as would be required under the null hypothesis that there is no systematic variation of the average cluster X-ray luminosity across the sky. Secondly, the motions of the XACIF and NOX samples in the outer shell differ by 2306 ± 846 km s $^{-1}$ and are inconsistent with each other at the 95% confidence level when no X-ray correction is applied to either subsample. Finally,

even when we consider the outer shell ACIF sample with no X-ray correction, we find that this sample is still marginally consistent with being at rest in the CMB frame (we would reject this at only the 89% confidence level). Thus, independent of the unknown X-ray correction to the NOX subsample, the evidence for flows beyond 6000 km s $^{-1}$ is weak.

Until all of these issues can be clarified by the addition of further X-ray data, we prefer the conservative conclusion that there is no evidence for large-amplitude large-scale motion beyond 6000 km s $^{-1}$.

Given the large random errors on the XACIF bulk motion, it would clearly be valuable to obtain X-ray data for a larger sample of the ACIF clusters. However, caution should be exercised before applying the L_m – α – L_X relation to still deeper cluster samples. Typical distance errors increase from $\approx 17\%$ at the median L_X in the XACIF sample to $\approx 30\%$ at highest X-ray luminosities due to the steepening of the L_m – α – L_X relation and the fact that L_X is distance-dependent. Consequently, extending the L_m – α – L_X relation in order to measure the bulk flow in larger volumes is expected to be doubly difficult. The results of Edge (1991) indicate that BCG metric luminosity is better correlated with X-ray temperature than with X-ray luminosity. Furthermore, the fractional distance error does not increase with T_X (whereas it does with L_X) because the X-ray temperature is distance-independent. A more promising approach would thus be to collect X-ray temperatures for a large all-sky sample of nearby clusters.

5. Conclusions

Using the subset of LP clusters which have X-ray luminosities from the XBACs sample of Ebeling *et al.* (1996) or from pointed ROSAT PSPC observations, we have shown that, for large- α BCGs, both the metric luminosities and residuals from the L_m – α relation are significantly correlated with the X-ray luminosity of the host cluster at the 99.6% confidence level.

We have included L_X as an additional parameter in the BCG relation and re-derived the bulk motion of the XACIF sample. Although we cannot rule out the possibility that the sample is at rest with respect to the CMB at better than the 98% confidence level, the motion of the XACIF sample is fully consistent with the lower amplitude (300 – 400 km s $^{-1}$) flows found by other workers (CFDW) on scales of 6000 km s $^{-1}$.

On larger scales ($cz_{LG} > 6000$ km s $^{-1}$), the ran-

dom errors in the derived bulk flow are large. The motion of XACIF sample is consistent with the most conservative hypothesis that these clusters are at rest in the CMB frame but also with the large amplitude motion found by LP. However, even when the X-ray data are excluded from the fit, the 107 clusters in the Lauer and Postman ACIF sample in the outer shell do not have a significant bulk motion with respect to the CMB. Furthermore, we note that use of the $L_m - \alpha - L_X$ relation introduces a systematic correction to the bulk flow of the XACIF sample which is comparable to the random errors and goes in the sense of reducing both the amplitude and the significance of its motion in the CMB frame. Had we used the $L_m - \alpha$ relation employed by LP, we would have incorrectly found that this sample had a highly significant (98.8%) motion with respect to the CMB. We would also have found that the bulk motions of the XACIF sample and the remainder of the LP sample disagreed by 2306 ± 846 km s $^{-1}$ which is significant at the 95% confidence level.

We conclude that the evidence for flows beyond 6000 km s $^{-1}$ is weak and that claims of large-scale, large-amplitude flows should be regarded with caution until further X-ray data become available.

We thank the authors of Ebeling *et al.* (1996), and there in particular Dr. H. Böhringer, for making their X-ray cluster sample available to us prior to publication. Thanks are also due to Alastair Edge for many helpful discussions and to F.D.A. Hartwick for comments on an earlier version of the manuscript. We are indebted to the referee, Marc Postman, whose criticism helped to improve this paper. HE acknowledges financial support from an EARA fellowship and SAO contract SV4-64008.

REFERENCES

Abell, G. O. 1958, ApJS, 3, 211

Abell, G. O., Corwin, H. G., & Olowin, R. P. 1989, ApJS, 70, 1 (ACO)

Bautz, L. P., & Morgan, W.W. 1970, ApJ, 162, 149 (BM)

Colless, M. 1995, AJ, 109, 1937

Courteau, S., Faber, S. M., Dressler, A., & Willick, J. A. 1993, ApJ, 412, 51 (CFDW)

Dalton, G. B., Efstathiou, G., Maddox, S. J., & Sutherland, W. J. 1994, MNRAS, 269, 151

Ebeling, H., Voges, W., Böhringer, H., Edge, A. C., Huchra, J. P., & Briel, U. G. 1996, MNRAS, 281, 799

Edge, A. C. 1991, MNRAS, 250, 103

Feldman, H. A., & Watkins, R. 1994, ApJ, 430, 17

Graham, A., Lauer, T. R., Colless, M., & Postman, M. 1996, preprint (astro-ph/9306006).

Gramann, M., Bahcall, N. A., Cen, R., & Gott, J. R. 1995, ApJ, 441, 449

Guzman, R., Lucey, J. R., & Bower, R. G. 1993, MNRAS, 265, 731

Hoessel, J. G. 1980, ApJ, 241, 493

Hoessel, J. G., & Schneider, D. P. 1985, AJ, 90, 1648

Humason, M. L., Mayall, N. U., & Sandage, A. R., 1956, AJ, 61, 97

Isobe, T., Feigelson, E. D., & Nelson, P. I. 1986, ApJ, 306, 490

Jaffe, A. H., & Kaiser, N. 1995, ApJ, 455, 26

James, P. A., Joseph, R. D., & Collins, C. A., 1987, MNRAS, 229, 53

Kormendy, J. 1977, ApJ218, 333

Lauer, T. R., & Postman M. 1994, ApJ, 425, 418 (LP)

Lucey, J. R. 1983, MNRAS, 204, 33P

Lucey, J. R., & Carter, D. 1988, MNRAS, 231, 15P

Lucey, J. R., Guzman, R., Carter, D., & Terlevich, R. J., 1988, MNRAS, 253, 584.

Peebles, P. J. E. 1968, ApJ, 153, 13

Postman, M., & Lauer, T. R. 1995, ApJ, 440, 28 (PL)

Sandage, A. 1972a, 173, 485

Sandage, A. 1972b, 178, 1

Sandage, A. 1975, ApJ, 202, 563

Scaramella, R., Zamorani, G., Vettolani, G., & Chincarini, G. 1991, AJ, 101, 342

Scott, E. L. 1957, AJ, 62, 248

Strauss, M. A., Cen, R., Ostriker, J. P., Lauer, T. R. & Postman, M. 1995, ApJ, 444, 507

Sutherland, W. 1988, MNRAS, 234, 159

van Haarlem, M. P. 1996, preprint (astro-ph/9601081)

Vettolani, G., Chincarini, G., Scaramella, R., & Zamorani, G. 1990, AJ99, 1709

Watkins, R., & Feldman, H. A. 1995, ApJ, 453, L73

Zabludoff, A. I., Geller, M. J., Huchra, J. P., & Vo-
geley, M. S. 1993, AJ, 106, 1273

TABLE 1
THE X-RAY-ABELL CLUSTER SAMPLE

Name	M_L	α_L	α'	$\log(L_{44})$	ΔM_L	σ_r
A0076	-22.493	0.55	-0.09	-0.50	0.110	0.151
A0119	-22.719	0.76	-0.21	0.12	-0.004	0.200
A0147	-22.493	0.42	-0.38	-0.69	-0.155	0.204
A0168	-22.535	0.57	-0.47	-0.36	0.087	0.169
A0193	-22.615	0.68	0.30	-0.21	0.058	0.169
A0194	-22.401	0.60	-0.72	-1.33	0.239	0.160
A0195	-22.398	0.46	-0.47	-1.24	0.014	0.229
A0262	-22.144	0.81	0.09	-0.56	0.342	0.250
A0376	-22.525	0.69	-0.30	-0.25	0.144	0.170
A0407	-22.314	0.84	-0.98	-0.70	0.056	0.111
A0496	-22.576	0.78	-0.51	0.12	0.141	0.209
A0533	-22.383	0.50	-0.34	-0.99	0.139	0.177
A0539	-22.362	0.50	-0.17	-0.39	0.172	0.155
A0548a	-22.453	0.49	-0.26	-0.51	0.061	0.164
A0569	-22.354	0.47	-0.81	-2.23	0.041	0.850
A0576	-22.058	0.29	-0.77	-0.25	-0.032	0.606
A0671	-22.934	0.71	-0.04	-0.45	-0.293	0.176
A0779	-22.946	0.59	-0.21	-1.46	-0.309	0.155
A0957	-22.821	0.76	-0.17	-0.53	-0.242	0.183
A1060	-22.176	0.80	-0.68	-0.76	0.271	0.132
A1139	-22.296	0.58	-0.30	-1.12	0.335	0.159
A1185	-22.458	0.61	-1.19	-0.94	0.186	0.167
A1314	-22.497	0.58	0.09	-0.80	0.134	0.147
A1367	-22.529	0.53	-0.85	-0.28	0.050	0.206
A1631a	-22.587	0.65	-0.60	-0.55	0.068	0.160
A1644	-22.704	0.98	-0.64	0.12	-0.083	0.425
A1656	-23.041	0.60	-0.47	0.45	-0.392	0.174
A1736	-23.118	0.58	-0.64	-0.06	-0.487	0.177
A1836	-22.679	0.58	-0.51	-1.50	-0.047	0.164
A1983	-22.311	0.34	-0.64	-0.71	-0.256	0.529
A2052	-22.557	0.89	-0.55	-0.02	0.046	0.244
A2063	-22.393	0.79	-0.85	-0.11	0.258	0.176
A2107	-22.863	0.77	-0.51	-0.28	-0.241	0.173
A2147	-22.370	0.66	-0.72	0.05	0.314	0.182
A2151	-22.412	0.75	-0.26	-0.37	0.210	0.179
A2197b	-23.011	0.59	-0.17	-1.51	-0.375	0.154
A2199	-22.769	0.78	-0.60	0.19	-0.035	0.216
A2572a	-22.605	0.53	0.30	-0.36	-0.027	0.131
A2589	-22.430	0.78	-0.17	-0.11	0.228	0.202
A2593	-22.509	0.80	-1.11	-0.36	0.061	0.137
A2634	-22.765	0.65	-0.26	-0.41	-0.104	0.162
A2657	-21.998	0.34	-0.60	-0.17	0.208	0.270
A2717	-22.342	0.91	0.21	-0.52	-0.088	0.694
A2877	-23.199	0.60	-0.30	-0.80	-0.556	0.159
A3144	-22.096	0.44	-0.30	-1.17	0.258	0.194

TABLE 1—*Continued*

Name	M_L	α_L	α'	$\log(L_{44})$	ΔM_L	σ_r
A3376	-22.615	0.61	-0.34	-0.11	0.038	0.164
A3389	-22.604	0.51	-0.47	-0.90	-0.061	0.187
A3395	-22.429	0.78	-0.60	0.02	0.262	0.197
A3526	-22.883	0.72	-0.64	-0.45	-0.248	0.156
A3528b	-22.934	0.67	-0.04	-0.30	-0.267	0.166
A3530	-22.861	0.76	0.09	-0.49	-0.272	0.207
A3532	-22.677	0.72	-0.09	0.03	0.021	0.182
A3556	-22.966	0.57	-0.43	-0.40	-0.344	0.167
A3558	-23.067	0.89	-0.60	0.37	-0.235	0.383
A3559	-22.926	0.62	0.00	-1.00	-0.280	0.156
A3562	-22.579	0.70	-0.26	0.07	0.120	0.179
A3565	-22.619	0.53	-0.21	-2.14	-0.048	0.164
A3571	-22.900	1.10	-0.89	0.44	0.081	0.422
A3574	-22.539	0.74	-0.09	-1.58	-0.113	0.172
A3581	-22.219	0.61	-0.30	-0.64	0.429	0.159
A3716	-22.567	0.71	-0.34	-0.35	0.085	0.169
A3733	-22.163	0.64	0.00	-0.81	0.485	0.160
A4038	-22.342	0.45	-0.38	-0.11	0.118	0.174
A4059	-22.908	0.89	-0.47	0.07	-0.254	0.273

NOTE.—The BCG is assumed to lie at a distance given by its velocity in the Local Group frame with $H_0 = 80 \text{ km s}^{-1} \text{ Mpc}^{-1}$. L_{44} is the X-ray luminosity in units of $10^{44} \text{ ergs s}^{-1}$ in the 0.1 – 2.4 keV band.